ACS SyntheticBiology

pubs.acs.org/synthbio

Research Article

Efficient Amber Suppression *via* Ribosomal Skipping for *In Situ* Synthesis of Photoconditional Nanobodies

Eike F. Joest, Christian Winter, Joshua S. Wesalo, Alexander Deiters, and Robert Tampé*

Cite This: *ACS Synth. Biol.* 2022, 11, 1466−1476

Read Online

ACCESS | Metrics & More | Article Recommendations | Supporting Information

ABSTRACT: Genetic code expansion is a versatile method for *in situ* synthesis of modified proteins. During mRNA translation, amber stop codons are suppressed to site-specifically incorporate non-canonical amino acids. Thus, nanobodies can be equipped with photocaged amino acids to control target binding on demand. The efficiency of amber suppression and protein synthesis can vary with unpredictable background expression, and the reasons are hardly understood. Here, we identified a substantial limitation that prevented synthesis of nanobodies with N-terminal modifications for light control. After systematic analyses, we hypothesized that nanobody synthesis was severely affected by ribosomal inaccuracy during the early phases of translation. To circumvent a background-causing read-through of a premature stop codon, we designed a new suppression concept based on ribosomal skipping. As an example, we generated intrabodies with photoactivated target binding in mammalian cells. The findings provide valuable insights into the genetic code expansion and describe a versatile synthesis route for the generation of modified nanobodies that opens up new perspectives for efficient site-specific integration of chemical tools. In the area of photopharmacology, our flexible intrabody concept builds an ideal platform to modulate target protein function and interaction.

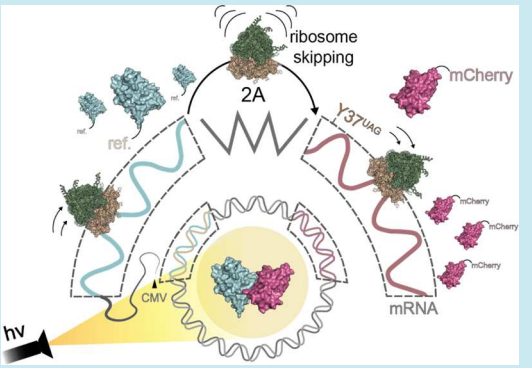

KEYWORDS: *genetic code expansion, intrabodies, optochemical biology, photoactivation, protein modification, photopharmacology*

INTRODUCTION

Conditional protein modifications are fundamental in the life sciences. Genetic code expansion connects the versatility of chemical synthesis to protein expression in living systems.[1−10] Protein modifications can be inserted site-specifically *via* natural translation machineries.[11] By reprogramming the genetic code, non-canonical amino acids bearing a modification of choice are used in ribosomal polypeptide synthesis.[12−14] Non-canonical amino acids have many applications in protein engineering, as they can be equipped with isotopes for structural studies,[15−17] photoreactive groups and post-translational modifications for functional studies,[18−29] reactive groups for bio-orthogonal coupling,[13,15,30−34] photocross-linkers,[1,22,35−40] infrared-active probes to follow conformational dynamics,[6,36−41] fluorescent dyes for imaging,[42−46] biotin analogues for high-affinity interactions with streptavidin,[47] and stable phosphotyrosine analogues for analysis of signal transduction.[23,48] Site-specific incorporation is achieved by suppressing a stop codon with an additional aminoacyl-tRNA-synthetase (aaRS)/tRNA pair.[4,14,49,50] In bacterial or mammalian cells, the rarest amber codon (TAG) is most often used to minimize suppression throughout the proteome.[5,6,12,33,51] However, the underlying processes of the genetic code expansion are complex and hardly understood.[6,7] For efficient protein synthesis, an ideal interplay of all chemical and biological components is required.[12,50] To date, no standard approach for the screening of optimal parameters is available. In mammalian cells, the *in vivo* synthesis of modified proteins is further challenged by the relatively high abundance (23%) of the amber codon, in contrast to only 9% in *Escherichia coli*.[52−54] The potential for incorporation in response to endogenous amber codons can be partially prevented by the cellular compartmentalization of the mRNA using liquid-phase segregation or membrane recruitment.[55,56] However, the problem of cells incorporating natural amino acids at TAG codons is well known, particularly for Phe and Tyr analogues. Though background-causing amino acids may be dropped out of the media in *E. coli*,[11,57] methods for addressing this problem in eukaryotic species have not been reported.

Here, we systematically identified a potential interference factor and reported a novel synthesis strategy to circumvent limitations for synthesis of modified nanobodies. After

Received: September 19, 2021
Published: January 21, 2022

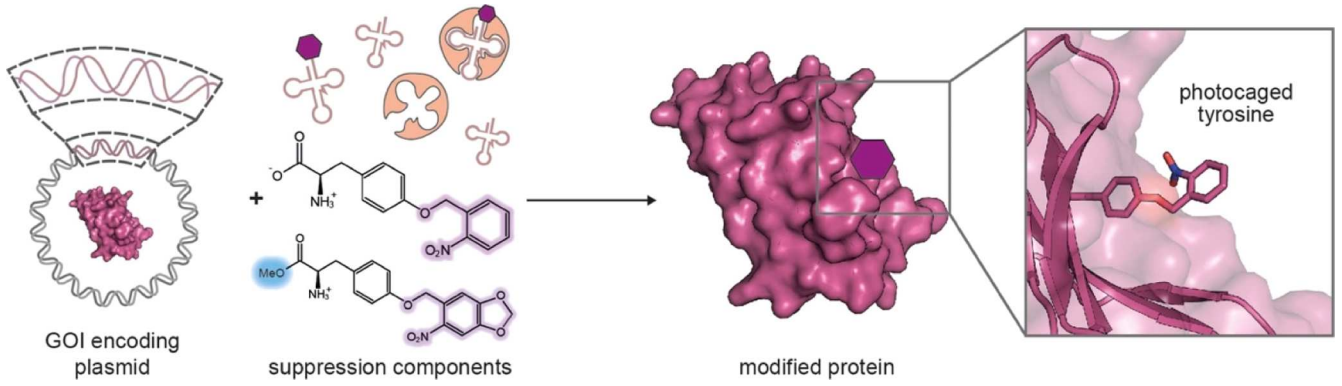

Figure 1. Genetic code expansion enables the synthesis of the modified proteins (pink). To generate the functionalized proteins in living cells, natural translation machineries are reprogrammed. Using an orthogonal aaRS/tRNA pair (beige), amber stop codons are suppressed to site-specifically introduce a non-canonical amino acid (magenta). For photoactivated binding, photocaged tyrosine analogous are introduced at position Tyr37 of the α-GFP nanobody (enhancer).

introducing an amber stop codon at a strategically defined position in the 5′ region of the gene of interest (GOI), we observed an inefficient termination of translation. The resulting background expression impeded the synthesis of the modified protein by genetic code expansion. A systematic analysis revealed frequent read-through across the premature stop codon. Recent studies using ribosome display technologies reported reduced accuracy in early phases of translation in the 5′ region.[58−61] We rationalized that premature amber stop codons in nanobodies are prone to such infidelity. For amber suppression with high efficiency, we present a new approach that improves the fidelity of ribosomal synthesis, particularly for amber stop codons present in the 5′ region of the mRNA.

As an outstanding example, we generated intrabodies with photoactivated binding to intracellular antigens. The strategy opens new avenues because intrabodies are ideal for imaging or modulating intracellular targets. Controlling the protein function with light enables experimental and therapeutic applications with minimal interference and high spatiotemporal precision. In general, genetic code expansion allows the synthesis of photoactivatable (PA) proteins.[21,26] To this end, amino acids equipped with large photolabile protection groups are site-specifically introduced at crucial positions. Active sites and interaction interfaces, for example, constitute excellent targets. In this context, we described the synthesis of a conditional interaction pair *via* a genetic code expansion in a stable human cell line.[62] To generalize the concept to other proteins and expression hosts and to reduce the amount of work required, it would be beneficial to avoid stable genomic integration. Moreover, synthesis based on transient transfection would facilitate flexible tagging to modulate the target protein.

RESULTS AND DISCUSSION

To generate a PA version of the α-GFP nanobody (enhancer), an amber mutation was introduced at position Tyr37.[63,64] Incorporation of a tyrosine analogue bearing a bulky photolabile protection group controls target binding (Figure 1). After photocleavage, the native paratope is restored, allowing rapid high-affinity binding of the target. For transient transfection, we cloned the construct in a plasmid for expression in mammalian cells (Figure 2a, construct I). To visualize protein synthesis, we used a C-terminal fusion to the red fluorescent protein mCherry. An engineered variant of the pyrrolysyl-tRNA (PylT) synthetase (PylRS) pair from *Methanosarcina barkeri* was co-transfected in order to suppress the premature amber stop codon.[26] First, we selected *ortho*-nitrobenzyl-caged tyrosine (ONBY) to replace Tyr37 (Figure 2b).[22] After transient transfection of HeLa cells, we analyzed the synthesis efficiency of the PA nanobody ($^{PA}Nb^{mCherry}$) *via* flow cytometry. The fluorescence intensities of cells expressing the unmodified (UM) construct ($^{UM}Nb^{mCherry}$) were used for normalization (Figure S1). After solely transfecting the $^{PA}Nb^{mCherry}$-encoding plasmid in the absence of ONBY, we observed up to 40% cells with similar fluorescence intensities.[11] High ratios of mCherry-positive cells indicated that the premature amber codon did not terminate mRNA translation in the absence of amber suppression components. In contrast, 30% positive cells were recorded under amber suppression conditions by co-transfecting $^{PA}Nb^{mCherry}$ with the orthogonal aaRS/tRNA pair and supplementing the medium with ONBY (Figure 2c). These results demonstrated insufficient suppression of the premature termination signal.

To improve amber suppression, we equipped the $^{PA}Nb^{mCherry}$ encoding plasmid with four additional copies of the orthogonal tRNA (PylT)[65,66] (Figure 2a, construct II). Here, 15% of mCherry-positive cells were observed under amber suppression conditions, and 20% after solely transfecting the plasmid in the absence of ONBY (Figure 2c). We excluded the background expression of unfused mCherry by replacing the start methionine with an alanine (Met1Ala) to eliminate the possibility that this could be used as a translational initiation site (Figure 2a, construct III). Again, high ratios of mCherry-positive cells were recorded in the absence of amber suppression components. To identify the source of mCherry fluorescence, we analyzed the translation products in the cell lysates by sodium dodecyl sulfate−polyacrylamide gel electrophoresis (SDS-PAGE) and in-gel fluorescence. We observed the full-length fusion construct $Nb^{mCherry}$ in all samples. Moreover, amber construct samples showed similar fluorescence intensities (Figure S2). These surprising results indicated that the amber stop codon $Tyr37^{TAG}$ failed to terminate translation efficiently. Consequently, the read-through caused a background protein expression, competing with efficient synthesis of the modifed protein.

One reason for insufficient termination of translation could be an unbalanced mRNA/tRNA ratio. To harmonize the RNA level, we cloned the constructs into a plasmid with a previously

https://doi.org/10.1021/acssynbio.1c00471
ACS Synth. Biol. 2022, 11, 1466−1476

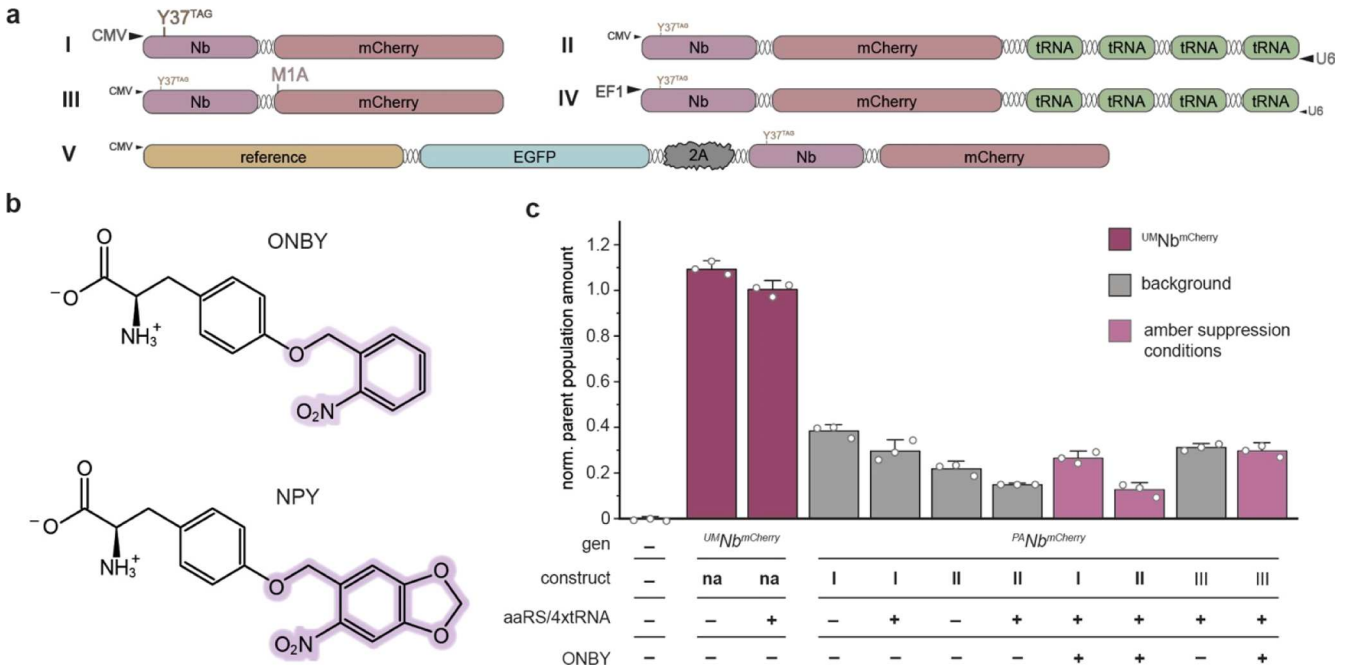

Figure 2. Synthesis of the modified protein in mammalian cells by amber suppression. (a) Expression cassettes for the generation of $^{PA}Nb^{mCherry}$ intrabodies by transient transfection. To site-specifically insert photocaged tyrosines (b), an amber codon was introduced at position Tyr37. For amber suppression, an orthogonal aaRS/4xtRNA pair was co-transfected. (c) Quantity of $Nb^{mcherry}$-positive cells after transient transfection of expression cassettes under the control of the CMV promoter (constructs I−III), monitored by flow cytometry. The premature amber codon at position Tyr37-inadequately terminated translation. Background expression limited sufficient amber suppression for the synthesis of $^{PA}Nb^{mCherry}$ (construct I). Efficient amber suppression was not achieved by encoding four additional copies of the orthogonal tRNA (construct II). The parallel synthesis of unfused mCherry was excluded by the substitution of the potential start codon with an mCherry-M1A mutation (construct III). aaRS/4xtRNA = NPYRS/4xPylT co-transfection, ONBY = medium supplemented with 0.25 mM ONBY. Living HeLa cells 24 h after transfection, mean amount of n = 3 biological replicates ± SD.

described design for amber suppression.[12,13,67] In this case, the GOI is under control of the strong EF-1 alpha promoter and amber suppression supported by four additional PylT copies (Figure 2a, construct IV). After transient transfection, we measured background expression by flow cytometry. Relative to the UM construct, up to 90% cells showed similar fluorescence intensities in the absence of suppression components (Figure S3). Again, the amber stop codon $Tyr37^{TAG}$ failed to terminate translation, indicating that altering the mRNA/tRNA ratio did not prevent an undesired read-through.

Recent advances in ribosome profiling and other technologies demonstrated reduced fidelity in early phases of translation.[58−61] We rationalized that the early amber codon at position Tyr37 is prone to such inaccuracy. In a recent study, we observed slightly increased amber suppression efficiency by using a bicistronic translation approach.[29] In order to circumvent the $Nb^{mCherry}$ background expression, we developed a new approach inspired by the translation strategy of the foot-and-mouth disease virus (Figure 1a, construct V). First, we implemented an upstream encoded GOI to our expression cassette to reduce translational slowdown and inaccuracy. To analyze $^{PA}Nb^{mCherry}$ binding, we co-expressed the cognate target protein (EGFP), which can be fused to many reference proteins *via* a multiple cloning site. As an initial reference, we used the ER-resident transporter associated with antigen processing (TAP1).[68,69] Second, we connected both gene constructs *via* the foot-and-mouth disease virus ribosomal skipping site (F2A), which allows bicistronic translation of two proteins (target and nanobody) in a single ribosome passage (Figure 3a).[29,70] Polycistronic mRNAs are a valuable strategy for the expression of certain genes in mammalian cells that is gaining increasing recognition.[71] Parallel protein synthesis was monitored using flow cytometry to detect the two fluorescent reporters (Figure S4). In the absence of amber suppression components, no mCherry-positive cells were detected (Figure 3b), while the expression of the GFP-tagged reference protein indicated efficient transient transfection (Figure S4). Gratifyingly, the new approach restored the translational stop function of the amber codon at position Tyr37. In contrast to all previous approaches (constructs I−IV), efficient amber suppression was observed after this complete silencing of the background expression. By suppressing the amber codon with ONBY, we observed up to 50% $Nb^{mCherry}$-positive cells (Figure 3b). To investigate the synthesis of $^{PA}Nb^{mCherry}$ with improved photodeprotection properties, we suppressed the amber codon with nitropiperonyl-caged tyrosine (NPY). After transfection, we observed 60% of cells that contained the PA intrabody (Figure 3b). Background expression was minimal in the absence of amber-suppression components. These results demonstrate high fidelity in amber suppression and photocaged tyrosine incorporation. Importantly, the upstream reference protein restored the functionality of the amber codon at position Tyr37 and allowed efficient genetic code expansion for the generation of photoconditional intrabodies. For simplicity, we termed the new plasmid p2A-Amber (Figure 3a).

In contrast to the synthesis in stable cell lines, expression by transient transfection is flexible toward other hosts, with no need for stable transfection and tedious selection. To scale up

https://doi.org/10.1021/acssynbio.1c00471
ACS Synth. Biol. 2022, 11, 1466−1476

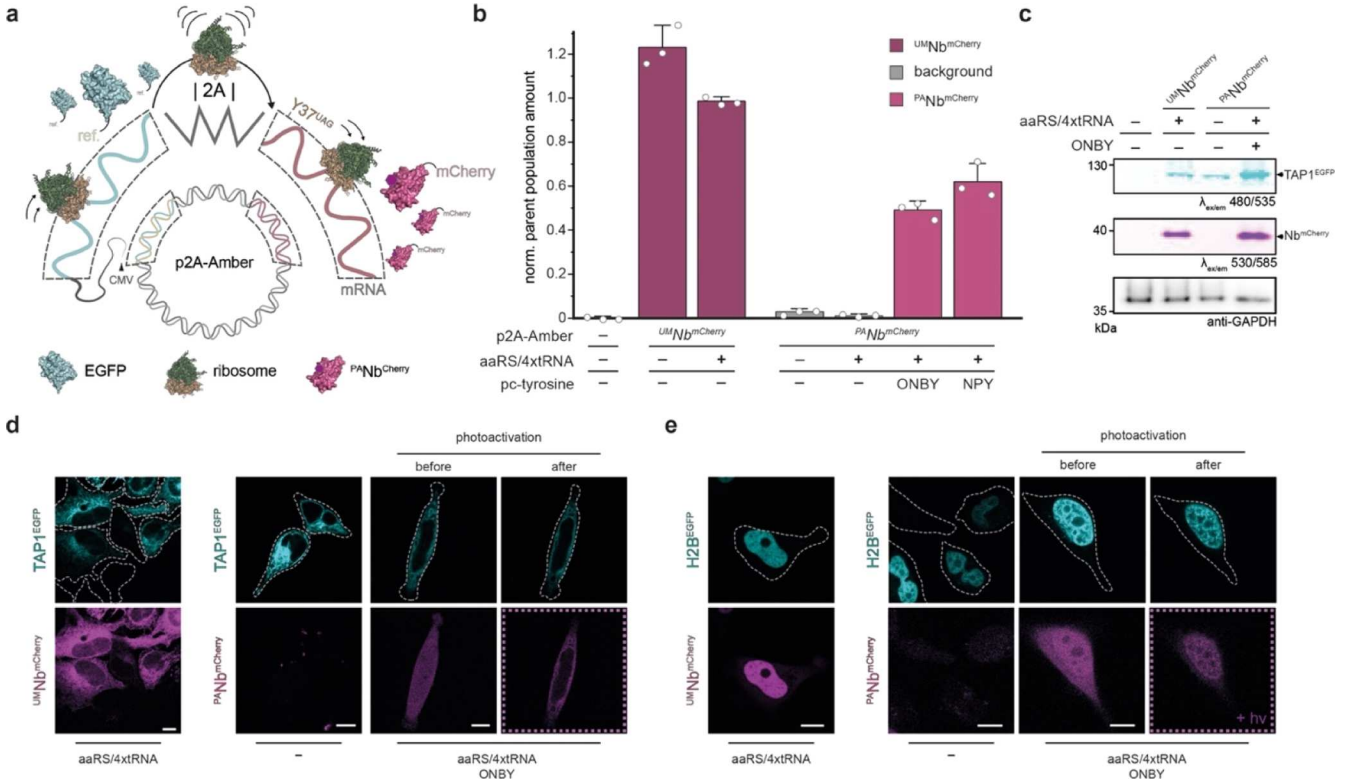

Figure 3. Synthesis of the modified protein in mammalian cells using p2A-Amber. (a) Plasmid design circumvents ribosomal inaccuracy in early phases of translation for efficient amber suppression by adding an upstream protein. As an example, the photoactivatable intrabody $^{PA}Nb^{mCherry}$ is generated. To facilitate intracellular binding analysis, a GFP-tagged reference protein was encoded upstream of the intrabody gene. The proteins are separated during translation *via* a viral ribosomal skipping (F2A) site. (b) Amber suppression in HeLa cells monitored by flow cytometry. The plasmid design of p2A-Amber restored the termination signal at the position Tyr37 of the $^{PA}Nb^{mCherry}$ gene. Thereby, efficient amber suppression generated site-specifically modified intrabodies by transient transfection. Relative to the unmodified (UM) protein $^{UM}Nb^{mCherry}$, high quantity of $^{PA}Nb^{mCherry}$-containing cells were observed *via* the C-terminal mCherry. Living HeLa cells 24 h after transfection, mean quantity of $n = 3$ biological replicates ± SD. (c) Large-scale synthesis of the modified proteins by HEK-F cells after the transient transfection of p2A-Amber. In-gel fluorescence of cell lysates (2.5 μg total protein), displaying efficient generation of $^{PA}Nb^{mCherry}$. Before SDS-PAGE, cells were analyzed by flow cytometry and $^{PA}Nb^{mCherry}$-containing cells were enriched. Importantly, in the absence of ONBY, no $^{PA}Nb^{mCherry}$ were observed. (d) *In situ* photoactivation of $^{PA}Nb^{mCherry}$ inside living cells. Intracellular binding of the ER resident reference protein $TAP1^{EGFP}$ was corroborated by co-localization. (e) Photoactivated $^{PA}Nb^{mCherry}$ binding of the reference histone protein $H2B^{EGFP}$. Imaging conditions were adjusted to the level of the fluorescent protein expression for cells transfected with $H2B^{EGFP}$ | F2A | $^{UM}Nb^{mCherry}$. (d,e) CLSM live-cell imaging of living HeLa cells. Scale bar = 10 μm. (b–e) Mammalian cells were transiently transfected with p2A-Amber containing the UM construct ($^{UM}Nb^{mCherry}$) or the genetic code expansion construct ($^{PA}Nb^{mCherry}$) with the premature amber codon at position Tyr37. For the suppression of the amber codon, cells were co-transfected with a plasmid encoding an orthogonal aaRS/tRNA pair (aaRS/4xtRNA) and the medium was supplemented with photocaged tyrosine (0.25 mM, ONBY).

the synthesis of the modified protein, we analyzed our p2A-Amber strategy in HEK293-F cells. After transient transfection, we enriched $^{PA}Nb^{mCherry}$-positive cells by flow cytometry and analyzed protein synthesis by SDS-PAGE (Figure S5). In-gel fluorescence showed high levels of $^{PA}Nb^{mCherry}$ and the reference protein ($TAP1^{EGFP}$) when ONBY was present. In the absence of ONBY components, the amber codon terminated the synthesis of the mCherry-tagged intrabody. The analysis further validated efficient translational processing and cleavage into the two proteins by the ribosomal skipping site (Figure 3c).

Next, we analyzed the functionality of the inserted protein modification. Using confocal laser scanning microscopy (CLSM), we visualized $^{PA}Nb^{mCherry}$ in living HeLa cells that were transiently transfected with our new p2A-Amber plasmids. Under amber suppression conditions with ONBY, we observed a homogeneous distribution of $^{PA}Nb^{mCherry}$ in the cytosol (Figure 3d,e). The results confirmed that the photocage blocked the high-affinity interaction with EGFP-tagged target proteins in comparison to the $^{UM}Nb^{mCherry}$ (Figure S6). Immediately after *in situ* photodeprotection, we detected $^{PA}Nb^{mCherry}$ binding of the antigen transport complex ($TAP1^{EGFP}$)[69] or histone H2B located at the ER membrane or the nucleus, respectively (Figure 3d,e). The same results were obtained by generating $^{PA}Nb^{mCherry}$ with NPY *via* a p2A-Amber-mediated amber suppression (Figure S7). Collectively, these results confirmed the efficient processing and synthesis of PA intrabodies *via* genetic code expansion and ribosomal skipping.

In general, synthesis of non-canonical amino acids is quite laborious, and material consumption for genetic code expansion is high. Especially for the purification of recombinantly expressed proteins to homogeneity, large quantities of non-canonical amino acids are required. To optimize amber suppression, we combined our p2A-Amber approach with a methyl ester NPY concept.[72,73] The generation of methyl esters promises enhanced membrane crossing and protein incorporation.[73] Accordingly, we synthesized the methyl ester of NPY (NPY-Me) and quantified genetic code expansion by flow cytometry (Figure S8a). By

https://doi.org/10.1021/acssynbio.1c00471
ACS Synth. Biol. 2022, 11, 1466–1476

using various concentrations of NPY and NPY-Me, we systematically identified the optimal concentrations for amber suppression. At high concentrations, NPY-Me seemed to be toxic. However, we observed that a 25-fold lower concentration of NPY-Me (only 10 μM) was sufficient to evoke more than 60% of NPY-mediated amber suppression (Figure S8). For large-scale expression studies, these results will help to significantly decrease the amount of the precious materials. These results pave the way for improved future applications of this versatile sterically bulky UAA that has excellent photophysical properties.[26]

CONCLUSIONS

We systematically identified a deadlock of a genetic code expansion with nanobodies/intrabodies and circumvented inefficient protein synthesis by a new translation strategy. In this context, we identified that an early amber stop codon is potentially prone to ribosomal infidelity during early phases of mRNA translation corresponding to the N-terminal region of the nascent chain. The resulting background expression can severely affect the efficiency of amber suppression. We sought to eliminate background by pre-starting translation with an upstream gene. Inspired by the translational strategy of the foot-and-mouth disease virus, we implemented a ribosomal skipping site to separate both proteins during translation. The new approach establishing plasmid p2A-Amber allowed synthesis of modified nanobodies/intrabodies in mammalian cells with high efficiency. Due to its productive translational initiation, the resulting mRNA is likely to be highly stable,[74] which will allow efficient expression of a variety of single-chain binders for genetic code expansion. Correspondingly, we generated photoactivatable intrabodies in mammalian cells, which targeted different proteins in the ER membrane and nucleus. Similar to the viral ribosome skipping site, N-terminal fusions with the STELLA-tag, the GCE-tag, ubiquitin, SUMO, and other ubiquitin-like proteins can be applied, which could allow efficient genetic code expansion in 5′-regions of the GOI.[75−77] However, some proteins are potentially affected by N-terminal fusions. For nanobodies, the N-terminus is located close to the interaction-mediating CDR loops, which limits the use of N-terminal fusions in general. Here, the p2A-Amber approach facilitates simple and efficient co-translation of the reference and target proteins, with no potentially interfering changes to the latter.

Photoactivatable intrabodies are ideal tools to monitor or modulate target proteins in living cells. We controlled binding by introducing a photocaged tyrosine into the interaction interface of the α-GFP enhancer nanobody ($^{PA}Nb^{mCherry}$). Previously, we reported synthesis of photoactivatable intrabodies in stable mammalian cell lines. The new synthesis route based on transient transfection allows flexible upgrades of $^{PA}Nb^{mCherry}$ with additional fusion tags for target protein modulation. For example, combining $^{PA}Nb^{mCherry}$ with a degradation signal will allow photoconditional protein knockdowns to study essential genes and complex pathways. Additionally, the plasmid set facilitates the expression in other cells and higher protein yields.

The direct contrast to our stable cell lines[62] reveals further details about underlying processes. Stable transfection enabled a background-free synthesis of the modified nanobody. In this case, gene expression was carefully controlled *via* tetracycline induction to generate nearly endogenous protein levels. By transient transfection, a strong overexpression is evoked. In the case of transient transfection using conventional expression plasmids, the high mRNA levels can increase the likelihood of read-through events. Accordingly, we observed the highest quantity of $Nb^{mCherry}$ in the absence of amber suppression components under these conditions (constructs I−IV). In the presence of an orthogonal aaRS/tRNA pair, a competition of read-through and amber suppression events further complicates the procedure. By implementing a bicistronic expression of an upstream encoded gene *via* p2A-Amber, this competition is shifted toward amber suppression events.

Antibody/nanobody drug conjugates offer a broad range of pharmaceutical applications. Our approach offers a direct route to photopharmacology[78,79] using therapeutic antibodies. For conjugate generation, efficient synthesis and precise modification are key requirements.[80,81] By using our p2A-Amber strategy, high quantity of site-specifically modified nanobodies can be expressed in human cells. Because our approach is customizable, it can be a robust route for the synthesis of nanobodies harboring other non-canonical amino acids for various applications such as bioconjugation.

In summary, we acquired new insights about genetic code expansion by amber suppression. We showed that an early amber codon in nanobodies is prone to translational read-through. Consequently, efficient incorporation of unnatural amino acids is impeded. The novel plasmid design p2A-Amber, inspired by the foot-and-mouth-disease virus, circumvents the limitation. Hence, pA2-Amber offers efficient synthesis of modified nanobodies or similar proteins. Our findings will help to expand the toolbox of genetic code expansion and allow new *in vivo* applications of chemically modified proteins.

MATERIALS AND METHODS

Molecular Biology. Enzymes for molecular biology were used by following the manufacturers' instructions. For DNA amplification by PCR, Phusion high-fidelity DNA polymerase was used. Ligation was performed using T4 DNA ligase. The mCherry-tagged α-GFP enhancer ($Nb^{mCherry}$) was previously cloned into pcDNA3.1(+) by PCR and restriction enzymes.[82] The amber mutation at position Tyr37 was inserted as previously described by site-directed mutagenesis using the following primer pair: fwd 5′-AGC ATG CGT TGG TA**G** CGT CAG GCA CCG-3′, rev 5′-CGG TGC CTG ACG **C**TA CCA ACG CAT GCT-3′ (mutation in bold).[62] For the generation of a pcDNA3.1(+) construct with additional tRNA copies (plasmid II), the plasmid SE323 with four PylT copies under the control of individual U6 promotors was used. The plasmid SE325 was kindly provided by Kathrin Lang (TU Munich).[13] All four tRNA genes were cloned by PCR and endonuclease restriction into pcDNA3.1(+) encoding $Nb^{mCherry}$ with the amber mutation at position Tyr37. For PCR, a primer pair introducing an upstream MfeI restriction site and a downstream Bpu10I restriction site was applied. *MfeI* fwd: 5′-GTG GCG <u>CAA TTG</u> GGG GAT ACG GGG AAA AGG-3′, *Bpu10I* rev: 5′-GCG GTG <u>CCT AAG</u> CGG CAC CGG AGC GAT CGC AGA T-3′ (restriction sites are underlined). The mCherry mutant Met1Ala (plasmid III) was generated by site-directed mutagenesis using the pcDNA3.1-(+) plasmid encoding $Nb^{mCherry}$ with amber mutation. Base-exchange was performed with the following primer pair: fwd 5′-GTT AGC AGC GGT ACC **GCG** GTG AGC AAG GGC GAG-3′ and rev 5′-CTC GCC CTT GCT CAC **CGC** GGT ACC GCT GCT AAC-3′ (mutation in bold). For cloning of the mammalian expression vector with additional tRNA copies

https://doi.org/10.1021/acssynbio.1c00471
ACS Synth. Biol. 2022, 11, 1466−1476

Scheme 1. Synthesis of NPY (1) and NPY-Me (2) *via* Reaction of a Dityrosine−Cu^{2+} Complex with *o*-NPBr and Removal of the Cu^{2+} by Heating with a Solution Containing Excess Ethylenediaminetetraacetic acid (EDTA)

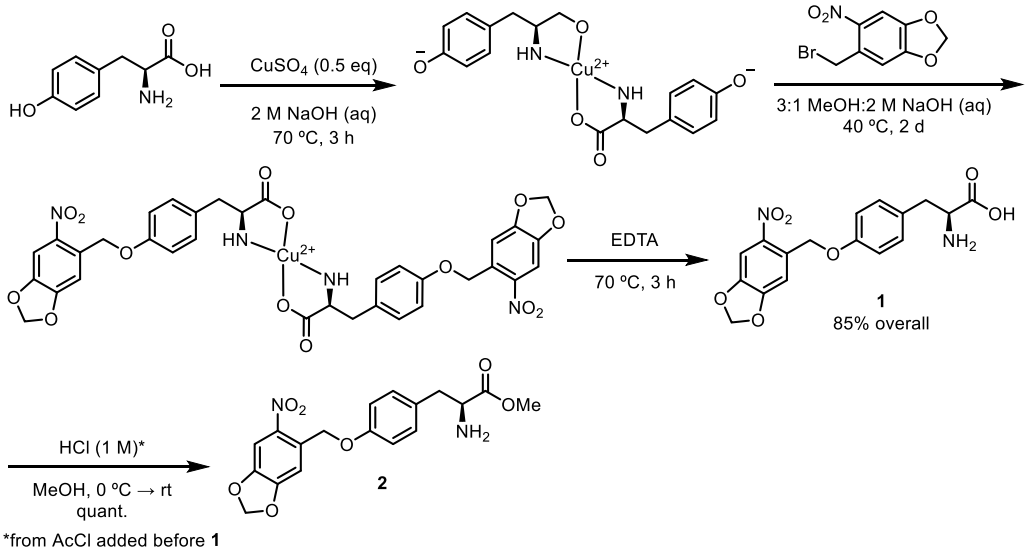

and a moderate EF-1 alpha promotor (plasmid IV), the $Nb^{mCherry}$ genes were cloned *via* endonuclease restriction into SE323 by exchanging a PylRS gene. Therefore, the UM $Nb^{mCherry}$ gene and the amber mutant encoded by pcDNA3.1-(+) were amplified by PCR using a primer pair that maintained an upstream NheI restriction site and inserted a downstream BamHI restriction site. *NheI* fwd: 5′-AGA CCC AAG CTG GCT AGC ACC-3′, *BamHI* rev 5′-GTG GCG GGA TCC GGT TTA AAC GGG CCC TCT AGA-3′ (restriction sites are underlined). A pcDNA3.1(+) plasmid encoding a multiple cloning site and downstream mEGFP| 2A |$Nb^{mCherry}$ with the amber mutation at position Tyr37 of the nanobody was designed for amber suppression after transient transfection (construct V, p2A-Amber). The plasmid was synthesized by GenScript. TAP1 or H2B was cloned into the multiple cloning site *via* endonuclease restriction. The TAP1 gene was amplified by PCR originating from a previously generated plasmid encoding $TAP1^{myc\text{-}SBP}$| 2A |$TAP2^{mVenus\text{-}His10}$.[29] A primer pair binding an upstream NheI restriction site and inserting a downstream BamHI restriction site was applied. *NheI* fwd: 5′-CCA AGC TGG CTA GCG TTT AAA CTT AAG CTT AGC-3′, *BamHI* rev: 5′-GCG GGC GCT CAC GGA TCC TTG TGG ACC ATC AGG AGC GTC AGC AGG AGC CTG GAC-3′ (restriction sites are underlined). Furthermore, the H2B gene for the generation of $H2B^{EGFP}$| 2A |$^{PA}Nb^{mCherry}$ was obtained by endonuclease restriction, based on a previously described plasmid encoding $H2B^{EGFP}$. The plasmid $H2B^{EGFP}$ in pEGFP-N1 was a gift from Geoffrey Wahl (Addgene #11680). After endonuclease restriction using HindIII upstream and BamHI downstream, the resulting frameshift was removed by site-directed mutagenesis using the following primer pair fwd: 5′-ACC AGC GCT AAG GAT CCA ATG GTG AGC AAG GGC GAG-3′ and rev: 5′-CTC GCC CTT GCT CAC CAT TGG ATC CTT AGC GCT GGT-3′ (insertion bold). For the generation of the UM intrabody ($^{UM}Nb^{mCherry}$), the amber mutation $Tyr37^{TAG}$ of the p2A-Amber constructs was exchanged toward the wild-type tyrosine by site-directed mutagenesis. The following primer pair with fwd 5′-CGT TAT AGC ATG CGT TGG TAT CGT CAG GCA CCG-3′ and rev 5′-ACG TTC TTT ACC CGG TGC CTG ACG ATA CCA ACG CAT GCT-3′ (mutation underlined) was used. The plasmid encoding the orthogonal aaRS/tRNA pair (NPYRS/4xPylT) was previously generated.[26,62] The pyrrolysine tRNA synthetase (PylRS) of *M. barkeri* contained the following mutations: L270F, L274M, N311G, and C313G.[26]

Synthesis and Analytics of Non-Canonical Amino Acids. NPY was synthesized using a procedure modified from a published report.[26] ONBY was purchased from Santa Cruz Biotechnology. Compound identity was validated by mass spectrometry (Figures S8−S11).

NPY-Me was synthesized as follows. All reagents and solvents were obtained from commercial suppliers and used without further purification. Reactions were monitored by thin-layer chromatography (TLC) using glass-backed silica gel (60 Å, F_{254}) plates (EMD Millipore). Flash chromatography was performed with silica gel (Sorbtech, 60 Å, 230−400 mesh). Nuclear magnetic resonance (NMR) spectra were obtained on 500 MHz or 600 MHz Bruker NMR spectrometers, and chemical shifts are in δ units (ppm) relative to the solvent signal. HRMS data were obtained using a Q Exactive Hybrid Quadrupole-Orbitrap mass spectrometer (Thermo Scientific) (Scheme 1).

o-Nitropiperonyl Bromide. This compound was synthesized by the Appel reaction according to literature procedures and was obtained as a yellowish tan solid in 90% yield (2.39 g, 9.19 mmol). Characterization data matched reported results.[83]

*(S)-2-Amino-3-(4-((6-nitrobenzo[d][1,3]dioxol-5-yl)-methoxy)phenyl)propanoic Acid (NPY, **1**).* A solution of copper sulfate pentahydrate (444.4 mg, 1.780 mmol, 0.5 equiv) in water (1.5 mL) was added dropwise to a stirred solution of L-tyrosine (645.0 mg, 3.564 mmol) in 2 M NaOH (2.8 mL, 5.6 mmol, 1.6 equiv) at 70 °C. After 1 h, the reaction mixture was cooled to 40 °C, and MeOH (10 mL) and additional 2 M NaOH (1.9 mL, 1.8 mmol, 0.5 equiv) was added. *o*-Nitropiperonyl bromide (984.1 mg, 3.784 mmol, 1.06 equiv) was added in 10 portions over 15 min. The mixture was stirred for 2 days at 40 °C in the exclusion of light (in a vial wrapped in aluminum foil). The mixture was centrifuged (500*g*, 1 min) and washed three times by resuspending in 1:3 MeOH/water

https://doi.org/10.1021/acssynbio.1c00471
ACS Synth. Biol. 2022, 11, 1466−1476

(10 mL) with a vortex mixer, repeating the centrifugation step, and discarding the supernatant. A solution of disodium EDTA dihydrate (796.6 mg, 2.140 mmol, 0.6 equiv) in water (10 mL) was added, and the mixture was stirred at 70 °C overnight. The product was cooled and was filtered in a funnel containing a glass frit and was washed with ice-cold water (20 mL) and ice-cold acetone (2 × 15 mL). The remaining solids were dried *in vacuo*, affording the product as a beige solid in a 85% yield overall (1.08 g, 3.01 mmol). Characterization data matched reported results.[26]

*Methyl (S)-2-Amino-3-(4-((6-nitrobenzo[d][1,3]dioxol-5-yl)methoxy)phenyl)propanoate (NPY-Me, **2**).* NPY (99.0 mg, 0.275 mmol) was added to a methanolic solution of 1 M HCl that had been prepared by adding AcCl (210 μL, 3.00 mmol) dropwise to anhydrous MeOH (3.0 mL) in a flame-dried vial on ice. The reaction mixture was allowed to warm to room temperature and was stirred overnight [note: TLC analysis (84:15:1 EtOAc/MeOH/Et_3N) of the reaction mixture shows a spurious spot at the baseline; a 1 M HCl in MeOH blank also produces this spot, suggesting that the solution destroys the TLC fluorescent indicator]. The reaction mixture was concentrated onto silica gel *in vacuo*. A silica gel column was neutralized by equilibration with 0.1% (v/v) Et_3N in EtOAc, and the sample was purified by flash chromatography (99:1 → 75:25 EtOAc/MeOH), affording the product as a pale yellow powder in quantitative yield (104.3 mg, 0.2789 mmol). ^{1}H NMR (600 MHz, DMSO-d_6): δ (ppm): 3.06 (m, 1H), 3.14 (m, 1H), 3.66 (s, 3H), 4.17 (t, J = 6.6 Hz, 1H), 5.35 (s, 2H), 6.26 (s, 2H), 6.96 (d, ^3J = 8.4 Hz, 2H), 7.17 (d, ^3J = 8.4 Hz, 2H), 7.26 (s, 1H), 7.74 (s, 1H), 8.74 (br s, 2H); ^{13}C NMR (151.1 MHz, DMSO-d_6): δ (ppm): 35.4, 53.0, 53.8, 67.0, 104.1, 106.0, 108.3, 115.4, 127.8, 130.5, 131.2, 141.8, 147.7, 152.6, 157.5, 169.9; HRMS-ESI (m/z) $[M + H]^+$ calcd for $C_{18}H_{19}O_7N_2$: 375.11868 Da, found 375.11741 Da.

Mass Spectrometry. Photocaged tyrosines, ONBY and NPY solved in phosphate buffered saline (PBS), were analyzed using a Waters BioAccord system running UNIFY 1.9.4. Individual samples were separated within an Acquity BEH C18 column (1.7 μm, 2.1 mm × 100 mm) and subjected to ESI-TOF mass spectrometry using a cone voltage of 30 V and capillary voltage of 0.8 kV in positive polarity.

Cell Culture. Adherent mammalian cells (HeLa, HEK293-F) were maintained in Dulbecco's modified Eagle medium (DMEM) containing 4.5 g/L glucose, supplied with 10% (v/v) fetal calf serum (FCS) in T75 cell culture flasks. For passaging, cells were detached by using PBS (Sigma-Aldrich) and 0.05% trypsin−EDTA (Gibco) every 2−3 days. Cells were cultivated in a tissue culture incubator at 37 °C and humidified with 5% CO_2. Following the established guidelines, mycoplasma contamination tests were regularly carried out.[84] For live-cell imaging of HeLa cells, 2.5 × 10^4 cells were seeded per glass-bottom 8-well imaging slide. For flow cytometry analysis of HeLa cells, 5 × 10^5 cells were seeded per 6-well, harvested using PBS and 0.05% trypsin−EDTA, washed once with DMEM and once with PBS. To establish suspension cultures of HEK293-F cells for high-scale synthesis of $^{PA}Nb^{mCherry}$, adherent cells were detached using PBS and 0.05% trypsin/0.02% EDTA/PBS. Cells were pelleted, washed in PBS (800 *g*, 5 min, RT), and resuspended in 100 mL of FreeStyle 293 medium. The suspension culture was incubated at 37 °C, 5% CO_2, and 125 rpm in 1 L Erlenmeyer flasks. For flow cytometry and cell sorting, cells were pelleted (800 g, 8 min, 4 °C) and washed twice with PBS before analysis.

Cell Transfection and Amber Suppression. For the expression analysis of the various plasmid I−V, HeLa cells were transiently transfected using Lipofectamine 2000 according to the manufacturer's instructions. Solubilized HEK293-F cells were transiently transfected using PEI for a large-scale expression. Two days before transfection, HEK293-F cultures were adjusted to 1 × 10^6 cells/mL. One day before transfection, cell concentrations were reduced to 0.5 × 10^6 cells/mL. For the transfection of a 100 mL culture, two mixtures were prepared. 100 μg of the plasmid (200 μg for co-transfection, 1:1 ratio) was diluted in 3.9 mL of Opti-MEM. In parallel, 400 μL of PEI (18 mM) was added to 3.25 mL of Opti-MEM. After 5 min, both solutions were mixed and incubated for 30 min at room temperature. For transfection, the solution was carefully added to the cell flasks. In order to ensure an optimal mixture, flasks were gently agitated during the procedure. To enable genetic code expansion by amber suppression, cells were co-transfected with the respective plasmids (constructs I−V, aaRS/4xtRNA), and 4−6 h later the medium was supplemented with non-canonical amino acids. For adherent cells, the medium was exchanged with DMEM, 4.5 g/L glucose, 10% (v/v) FCS, containing 250 μM ONBY or NPY, respectively. Stock solutions of the non-canonical amino acids were prepared in 100 mM NaOH and sterile-filtered. After stock addition to DMEM medium, the pH was neutralized by the same volume of 100 mM sterile-filtered HCl. NPY-Me was dissolved in dry DMSO at 50 mM to generate a stock solution. For suspension HEK293-F cultures, stocks of non-canonical amino acid and HCl were added in parallel to the cells cultured in the FreeStyle 293 medium. Again, flasks were gently agitated during the procedure. For optimal amber suppression, cells were cultivated in the corresponding medium for 24−48 h after transfection.

Flow Cytometry and Analysis. To analyze the synthesis of the modified proteins, the C-terminal mCherry tag was recorded *via* flow cytometry. For quantification, amounts of cells showing fluorescence intensities similar to the UM intrabody were used. Samples were recorded in biological triplicates by fluorescent-activated cell sorting (FACSMelody, BD Biosciences). mCherry fluorescence was excited with a 561 nm laser line and passed through a 613/18/LP605/10 filter set. To all samples, standard gates for doublet discrimination were applied. Flow cytometry data were evaluated using FlowJo 10.6.2 (BD), with the cell count of a mCherry transfection gate evaluated and plotted in OriginPro 2020 (OriginLab). For amber suppression efficiency analysis, the cell portions of the doublet-discriminated cells in the amber-supression gate were background corrected and normalized to the highest applied NPY concentration. Background correction was performed with a UAA-free sample. For the sorting of HEK293-F cells showing mCherry fluorescence in the range of $^{UM}Nb^{mCherry}$, a 100 mL culture was used.

Fluorescence Microscopy and Intrabody Photoactivation. For live cell CLSM imaging, cells cultivated in 8-well cell culture chambers were rinsed once and covered with a Ringer's solution (145 mM NaCl, 5 mM KCl, 2 mM $CaCl_2$, 1 mM $MgCl_2$, 10 mM HEPES, 10 mM glucose, pH 7.4). During imaging, chambers were incubated at 37 °C and humidified with 5% CO_2. Images were acquired by a confocal laser-scanning microscope (Zeiss LSM 880) combined with a Plan-Apochromat 63x/1.4 Oil DIC objective. Excitation of EGFP was achieved by using a 488 nm argon laser and of mCherry by a 543 nm helium-neon laser. To exclude fluorescence cross-

https://doi.org/10.1021/acssynbio.1c00471
ACS Synth. Biol. 2022, 11, 1466−1476

talk, sequential track imaging was used. For photoactivation of $^{PA}Nb^{mCherry}$, a bleaching function with 250 iterations, 50 cycles using a 405 nm diode (4.5 mW/μm^2) was applied. The whole region of interest was illuminated.

In-Gel Fluorescence and Immunoblotting. Synthesis of $^{UM/PA}Nb^{mCherry}$ was analyzed by in-gel fluorescence. To visualize the expression in adherent cells, HeLa cells were transiently transfected in 6-well plates. 5×10^5 cells were seeded in a 6-well plate. After 24 h, transient transfection using Lipofectamine 2000 was performed to initialize amber suppression. Cells were harvested on the following day by using PBS/0.05% trypsin−EDTA. The samples were pelleted (800 *g*, 4 °C) and washed once with DMEM to remove trypsin and once in PBS. For suspension HEK293-F cells, two PBS washing steps were applied. The obtained pellets were lysed in RIPA buffer containing 1% (v/v) benzonase and 1% (v/v) protease-inhibitor mix HP. The pellet of one 6-well plate was incubated in 30 μL of lysis buffer for 1 h (end-over-end rotation, RT). For HEK293-F cells, 100 μL lysis buffer was used. Subsequently, lysates were centrifuged (21,000 *g*, 30 min, 4 °C) and the supernatant collected. The obtained lysate protein concentration was determined by the Bradford assay (Pierce Detergent Compatible Bradford Assay Kit). To analyze the size of the synthesized protein by in-gel fluorescence, lysates were separated by discontinuous Tris/glycine SDS-PAGE (12%). Samples were prepared using a fivefold loading buffer concentrate with 30% (v/v) glycerol, 10% (w/v) SDS, 0.02% (w/v) Bromophenol Blue, and 250 mM Tris/HCl pH 6.8. After electrophoresis, the gel was washed three times with ddH_2O. In-gel fluorescence was analyzed using a gel and blot imaging system (Fusion FX imaging system, Vilber). EGFP was excited with 480 nm and detected using a 535 nm narrow band pass filter. For the detection of mCherry, a 530 nm and a 585 nm narrow band pass filter was used. As a loading control for in-gel fluorescence, an anti-GAPDH immunoblotting was performed. After imaging the samples, gels were semi-dry blotted on nitrocellulose membranes. The membranes were blocked in TBS-T supplemented with a 5% (w/v) skim milk powder (1 h, RT). Subsequently, membranes were washed three times in TBS-T. For immediate GAPDH detection, Direct-Blot HRP anti-GAPDH antibody was diluted 1:2000 in blocking buffer. Antibodies and membranes were incubated overnight at 4 °C. Before analysis, three washing steps with TBS-T were applied to remove unbound antibodies. For the chemiluminescent detection of the HRP conjugate, an ECL solution (Clarity Western ECL Substrate, Bio-Rad) was used in a gel and blot imaging system (Fusion FX imaging system, Vilber).

■ ASSOCIATED CONTENT

Supporting Information

The Supporting Information is available free of charge at https://pubs.acs.org/doi/10.1021/acssynbio.1c00471.

Experimental methods; experimental data; experimental approaches; gating strategies for flow cytometry quantification of $^{UM/PA}Nb^{mCherry}$ synthesis using the various constructs (I−V); in-gel fluorescence analysis highlighting translational read-through across amber mutation close to N-terminus; flow cytometry analysis of $^{UM/PA}Nb^{mCherry}$ synthesis *via* the EF1 promotor (construct IV); flow cytometry data of large-scale $^{UM/PA}Nb^{mCherry}$ synthesis by the transient transfection of solubilized mammalian cells using p2A-Amber; live cell CLSM controls showing constitutive $^{UM}Nb^{mCherry}$ target binding before and after light exposure; live-cell CLSM photoactivation of $^{PA}Nb^{mCherry}$ *via* NPY; NPY-Me-mediated $^{PA}Nb^{mCherry}$ synthesis monitored by flow cytometry; live-cell CLSM photoactivation of NPY-Me-synthesized $^{PA}Nb^{mCherry}$; and mass spectrometric analysis of ONBY, NPY, and NPY-Me compounds (PDF)

■ AUTHOR INFORMATION

Corresponding Author

Robert Tampé − *Institute of Biochemistry, Biocenter, Goethe University Frankfurt, 60438 Frankfurt/M, Germany;* orcid.org/0000-0002-0403-2160; Email: tampe@em.uni-frankfurt.de

Authors

Eike F. Joest − *Institute of Biochemistry, Biocenter, Goethe University Frankfurt, 60438 Frankfurt/M, Germany*

Christian Winter − *Institute of Biochemistry, Biocenter, Goethe University Frankfurt, 60438 Frankfurt/M, Germany*

Joshua S. Wesalo − *Department of Chemistry, University of Pittsburgh, Pittsburgh, Pennsylvania 15260, USA*

Alexander Deiters − *Department of Chemistry, University of Pittsburgh, Pittsburgh, Pennsylvania 15260, USA*

Complete contact information is available at: https://pubs.acs.org/10.1021/acssynbio.1c00471

Author Contributions

E.J. cloned the various constructs, performed amber suppression experiments, and imaged the cells by CLSM. FACS analysis was done by C.W. and E.J. C.W. performed mass spectrometric analyses of the various compounds. E.J., C.W., and R.T. carried out the data analysis. Photocaged amino acids were generated by J.S.W. and the synthesis was supervised by A.D. E.J. and R.T. wrote the manuscript with contributions from all authors. R.T. conceived and supervised the project.

Notes

The authors declare no competing financial interest.

■ ACKNOWLEDGMENTS

We thank Dr. Ralph Wieneke, Prof. Dr. Kathrin Lang (TU Munich), Holger Heinemann, and the entire lab for helpful discussions. We further thank Katharina Lindt for cell culture support. The German Research Foundation (GRK 1986, TA157/12-1, and CRC 807 to R.T.), the Volkswagen Foundation (Az. 96 496 to R.T.), the National Science Foundation (CHE-1904972 to A.D.), and the National Institutes of Health (R01GM132565 to A.D.) supported this work.

■ REFERENCES

(1) Chin, J. W.; Cropp, T. A.; Anderson, J. C.; Mukherji, M.; Zhang, Z.; Schultz, P. G. An expanded eukaryotic genetic code. *Science* **2003**, *301*, 964−967.

(2) Xie, J.; Schultz, P. G. An expanding genetic code. *Methods* **2005**, *36*, 227−238.

(3) Wang, L.; Brock, A.; Herberich, B.; Schultz, P. G. Expanding the genetic code of *Escherichia coli*. *Science* **2001**, *292*, 498−500.

(4) Hancock, S. M.; Uprety, R.; Deiters, A.; Chin, J. W. Expanding the genetic code of yeast for incorporation of diverse unnatural amino

acids via a pyrrolysyl-tRNA synthetase/tRNA pair. *J. Am. Chem. Soc.* **2010**, *132*, 14819−14824.
(5) Lang, K.; Chin, J. W. Cellular incorporation of unnatural amino acids and bioorthogonal labeling of proteins. *Chem. Rev.* **2014**, *114*, 4764−4806.
(6) Zhou, W.; Wesalo, J. S.; Liu, J.; Deiters, A. Genetic code expansion in mammalian cells: a plasmid system comparison. *Bioorg. Med. Chem.* **2020**, *28*, 115772.
(7) Brown, W.; Liu, J.; Deiters, A. Genetic code expansion in animals. *ACS Chem. Biol.* **2018**, *13*, 2375−2386.
(8) Wang, Q.; Parrish, A. R.; Wang, L. Expanding the genetic code for biological studies. *Chem. Biol.* **2009**, *16*, 323−336.
(9) de la Torre, D.; Chin, J. W. Reprogramming the genetic code. *Nat. Rev. Genet.* **2021**, *22*, 169−184.
(10) Shandell, M. A.; Tan, Z.; Cornish, V. W. Genetic code expansion: A brief history and perspective. *Biochemistry* **2021**, *60*, 3455−3469.
(11) Wang, Y.-S.; Fang, X.; Wallace, A. L.; Wu, B.; Liu, W. R. A rationally designed pyrrolysyl-tRNA synthetase mutant with a broad substrate spectrum. *J. Am. Chem. Soc.* **2012**, *134*, 2950−2953.
(12) Elsässer, S. J.; Ernst, R. J.; Walker, O. S.; Chin, J. W. Genetic code expansion in stable cell lines enables encoded chromatin modification. *Nat. Methods* **2016**, *13*, 158−164.
(13) Uttamapinant, C.; Howe, J. D.; Lang, K.; Beránek, V.; Davis, L.; Mahesh, M.; Barry, N. P.; Chin, J. W. Genetic code expansion enables live-cell and super-resolution imaging of site-specifically labeled cellular proteins. *J. Am. Chem. Soc.* **2015**, *137*, 4602−4605.
(14) Gubbens, J.; Kim, S. J.; Yang, Z.; Johnson, A. E.; Skach, W. R. In vitro incorporation of nonnatural amino acids into protein using tRNACys-derived opal, ochre, and amber suppressor tRNAs. *RNA* **2010**, *16*, 1660−1672.
(15) Liu, W.; Brock, A.; Chen, S.; Chen, S.; Schultz, P. G. Genetic incorporation of unnatural amino acids into proteins in mammalian cells. *Nat. Methods* **2007**, *4*, 239−244.
(16) Xie, J.; Wang, L.; Wu, N.; Brock, A.; Spraggon, G.; Schultz, P. G. The site-specific incorporation of p-iodo-L-phenylalanine into proteins for structure determination. *Nat. Biotechnol.* **2004**, *22*, 1297−1301.
(17) Hayashi, A.; Hino, N.; Kobayashi, T.; Arai, R.; Shirouzu, M.; Yokoyama, S.; Sakamoto, K. Dissecting cell signaling pathways with genetically encoded 3-iodo-L-tyrosine. *ChemBioChem* **2011**, *12*, 387−389.
(18) Wu, N.; Deiters, A.; Cropp, T. A.; King, D.; Schultz, P. G. A genetically encoded photocaged amino acid. *J. Am. Chem. Soc.* **2004**, *126*, 14306−14307.
(19) Chen, P. R.; Groff, D.; Guo, J.; Ou, W.; Cellitti, S.; Geierstanger, B. H.; Schultz, P. G. A facile system for encoding unnatural amino acids in mammalian cells. *Angew. Chem.* **2009**, *121*, 4112−4115.
(20) Tsai, Y.-H.; Essig, S.; James, J. R.; Lang, K.; Chin, J. W. Selective, rapid and optically switchable regulation of protein function in live mammalian cells. *Nat. Chem.* **2015**, *7*, 554−561.
(21) Chou, C.; Young, D. D.; Deiters, A. A light-activated DNA polymerase. *Angew. Chem.* **2009**, *121*, 6064−6067.
(22) Deiters, A.; Groff, D.; Ryu, Y.; Xie, J.; Schultz, P. G. A genetically encoded photocaged tyrosine. *Angew. Chem., Int. Ed.* **2006**, *45*, 2728−2731.
(23) Lemke, E. A.; Summerer, D.; Geierstanger, B. H.; Brittain, S. M.; Schultz, P. G. Control of protein phosphorylation with a genetically encoded photocaged amino acid. *Nat. Chem. Biol.* **2007**, *3*, 769−772.
(24) Peters, F. B.; Brock, A.; Wang, J.; Schultz, P. G. Photocleavage of the polypeptide backbone by 2-nitrophenylalanine. *Chem. Biol.* **2009**, *16*, 148−152.
(25) Arbely, E.; Torres-Kolbus, J.; Deiters, A.; Chin, J. W. Photocontrol of tyrosine phosphorylation in mammalian cells via genetic encoding of photocaged tyrosine. *J. Am. Chem. Soc.* **2012**, *134*, 11912−11915.
(26) Luo, J.; Torres-Kolbus, J.; Liu, J.; Deiters, A. Genetic encoding of photocaged tyrosines with improved light-activation properties for the optical control of protease function. *ChemBioChem* **2017**, *18*, 1442−1447.
(27) Jedlitzke, B.; Yilmaz, Z.; Dörner, W.; Mootz, H. D. Photobodies: light-activatable single-domain antibody fragments. *Angew. Chem., Int. Ed.* **2020**, *59*, 1506−1510.
(28) Jedlitzke, B.; Mootz, H. D. Photocaged nanobodies delivered into cells for light activation of biological processes. *ChemPhotoChem* **2021**, *5*, 22−25.
(29) Brunnberg, J.; Herbring, V.; Castillo, E. G.; Krüger, H.; Wieneke, R.; Tampé, R. Light control of the peptide-loading complex synchronizes antigen translocation and MHC I trafficking. *Commun. Biol.* **2021**, *4*, 430.
(30) Fleissner, M. R.; Brustad, E. M.; Kalai, T.; Altenbach, C.; Cascio, D.; Peters, F. B.; Hideg, K.; Peuker, S.; Schultz, P. G.; Hubbell, W. L. Site-directed spin labeling of a genetically encoded unnatural amino acid. *Proc. Natl. Acad. Sci. U.S.A.* **2009**, *106*, 21637−21642.
(31) Zeng, H.; Xie, J.; Schultz, P. G. Genetic introduction of a diketone-containing amino acid into proteins. *Bioorg. Med. Chem. Lett.* **2006**, *16*, 5356−5359.
(32) Saal, K.-A.; Richter, F.; Rehling, P.; Rizzoli, S. O. Combined use of unnatural amino acids enables dual-color super-resolution imaging of proteins via click chemistry. *ACS Nano* **2018**, *12*, 12247−12254.
(33) Heil, C. S.; Rittner, A.; Goebel, B.; Beyer, D.; Grininger, M. Site-specific labelling of multidomain proteins by amber codon suppression. *Sci. Rep.* **2018**, *8*, 14864.
(34) Aloush, N.; Schvartz, T.; König, A. I.; Cohen, S.; Brozgol, E.; Tam, B.; Nachmias, D.; Ben-David, O.; Garini, Y.; Elia, N.; Arbely, E. Live cell imaging of bioorthogonally labelled proteins generated with a single pyrrolysine tRNA gene. *Sci. Rep.* **2018**, *8*, 14527.
(35) Chin, J. W.; Martin, A. B.; King, D. S.; Wang, L.; Schultz, P. G. Addition of a photocrosslinking amino acid to the genetic code of Escherichia coli. *Proc. Natl. Acad. Sci. U.S.A.* **2002**, *99*, 11020−11024.
(36) Grunbeck, A.; Huber, T.; Abrol, R.; Trzaskowski, B.; Goddard, W. A., III; Sakmar, T. P. Genetically encoded photo-cross-linkers map the binding site of an allosteric drug on a G protein-coupled receptor. *ACS Chem. Biol.* **2012**, *7*, 967−972.
(37) Grunbeck, A.; Huber, T.; Sachdev, P.; Sakmar, T. P. Mapping the ligand-binding site on a G protein-coupled receptor (GPCR) using genetically encoded photocrosslinkers. *Biochemistry* **2011**, *50*, 3411−3413.
(38) Ye, S.; Zaitseva, E.; Caltabiano, G.; Schertler, G. F. X.; Sakmar, T. P.; Deupi, X.; Vogel, R. Tracking G-protein-coupled receptor activation using genetically encoded infrared probes. *Nature* **2010**, *464*, 1386−1389.
(39) Naganathan, S.; Ye, S.; Sakmar, T. P.; Huber, T. Site-specific epitope tagging of G protein-coupled receptors by bioorthogonal modification of a genetically encoded unnatural amino acid. *Biochemistry* **2013**, *52*, 1028−1036.
(40) Huber, T.; Naganathan, S.; Tian, H.; Ye, S.; Sakmar, T. P. Unnatural amino acid mutagenesis of GPCRs using amber codon suppression and bioorthogonal labeling. *Methods Enzymol.* **2013**, *520*, 281−305.
(41) Kang, H. J.; Baker, E. N. Intramolecular isopeptide bonds: protein crosslinks built for stress? *Trends Biochem. Sci.* **2011**, *36*, 229−237.
(42) Wang, W.; Li, H.; Wang, J.; Zu, L. Enantioselective organocatalytic tandem Michael−Aldol reactions: One-pot synthesis of chiral thiochromenes. *J. Am. Chem. Soc.* **2006**, *128*, 10354−10355.
(43) Summerer, D.; Chen, S.; Wu, N.; Deiters, A.; Chin, J. W.; Schultz, P. G. A genetically encoded fluorescent amino acid. *Proc. Natl. Acad. Sci. U.S.A.* **2006**, *103*, 9785−9789.
(44) Charbon, G.; Wang, J.; Brustad, E.; Schultz, P. G.; Horwich, A. L.; Jacobs-Wagner, C.; Chapman, E. Localization of GroEL determined by in vivo incorporation of a fluorescent amino acid. *Bioorg. Med. Chem. Lett.* **2011**, *21*, 6067−6070.

https://doi.org/10.1021/acssynbio.1c00471
ACS Synth. Biol. 2022, 11, 1466−1476

(45) Charbon, G.; Brustad, E.; Scott, K. A.; Wang, J.; Løbner-Olesen, A.; Schultz, P. G.; Jacobs-Wagner, C.; Chapman, E. Subcellular protein localization by using a genetically encoded fluorescent amino acid. *ChemBioChem* **2011**, *12*, 1818−1821.
(46) Chatterjee, A.; Guo, J.; Lee, H. S.; Schultz, P. G. A genetically encoded fluorescent probe in mammalian cells. *J. Am. Chem. Soc.* **2013**, *135*, 12540−12543.
(47) Hohl, A.; Mideksa, Y. G.; Karan, R.; Akal, A.; Vogler, M.; Groll, M.; Rueping, M.; Lang, K.; Feige, M. J.; Eppinger, J. Genetically encoded biotin analogues: Incorporation and application in bacterial and mammalian cells. *ChemBioChem* **2019**, *20*, 1795−1798.
(48) Xie, J.; Supekova, L.; Schultz, P. G. A genetically encoded metabolically stable analogue of phosphotyrosine in Escherichia coli. *ACS Chem. Biol.* **2007**, *2*, 474−478.
(49) Drabkin, H. J.; Park, H. J.; RajBhandary, U. L. Amber suppression in mammalian cells dependent upon expression of an Escherichia coli aminoacyl-tRNA synthetase gene. *Mol. Cell. Biol.* **1996**, *16*, 907−913.
(50) Serfling, R.; Lorenz, C.; Etzel, M.; Schicht, G.; Böttke, T.; Mörl, M.; Coin, I. Designer tRNAs for efficient incorporation of non-canonical amino acids by the pyrrolysine system in mammalian cells. *Nucleic Acids Res.* **2018**, *46*, 1−10.
(51) Lang, K.; Davis, L.; Torres-Kolbus, J.; Chou, C.; Deiters, A.; Chin, J. W. Genetically encoded norbornene directs site-specific cellular protein labelling via a rapid bioorthogonal reaction. *Nat. Chem.* **2012**, *4*, 298−304.
(52) Mitra, N. Incorporating unnatural amino acids into recombinant proteins in living cells. *Mater. Methods* **2013**, *3*, 1.
(53) Neumann, H.; Wang, K.; Davis, L.; Garcia-Alai, M.; Chin, J. W. Encoding multiple unnatural amino acids via evolution of a quadruplet-decoding ribosome. *Nature* **2010**, *464*, 441−444.
(54) Fredens, J.; Wang, K.; de la Torre, D.; Funke, L. F. H.; Robertson, W. E.; Christova, Y.; Chia, T.; Schmied, W. H.; Dunkelmann, D. L.; Beránek, V.; Uttamapinant, C.; Llamazares, A. G.; Elliott, T. S.; Chin, J. W. Total synthesis of *Escherichia coli* with a recoded genome. *Nature* **2019**, *569*, 514−518.
(55) Reinkemeier, C. D.; Girona, G. E.; Lemke, E. A. Designer membraneless organelles enable codon reassignment of selected mRNAs in eukaryotes. *Science* **2019**, *363*, No. eaaw2644.
(56) Reinkemeier, C. D.; Lemke, E. A. Dual film-like organelles enable spatial separation of orthogonal eukaryotic translation. *Cell* **2021**, *184*, 4886−4903.
(57) Fottner, M.; Brunner, A.-D.; Bittl, V.; Horn-Ghetko, D.; Jussupow, A.; Kaila, V. R. I.; Bremm, A.; Lang, K. Site-specific ubiquitylation and SUMOylation using genetic-code expansion and sortase. *Nat. Chem. Biol.* **2019**, *15*, 276−284.
(58) Dana, A.; Tuller, T. Determinants of translation elongation speed and ribosomal profiling biases in mouse embryonic stem cells. *PLoS Comput. Biol.* **2012**, *8*, No. e1002755.
(59) Sharma, A. K.; Sormanni, P.; Ahmed, N.; Ciryam, P.; Friedrich, U. A.; Kramer, G.; O'Brien, E. P. A chemical kinetic basis for measuring translation initiation and elongation rates from ribosome profiling data. *PLoS Comput. Biol.* **2019**, *15*, No. e1007070.
(60) Riba, A.; Di Nanni, N.; Mittal, N.; Arhné, E.; Schmidt, A.; Zavolan, M. Protein synthesis rates and ribosome occupancies reveal determinants of translation elongation rates. *Proc. Natl. Acad. Sci. U.S.A.* **2019**, *116*, 15023−15032.
(61) Gobet, C.; Naef, F. Ribosome profiling and dynamic regulation of translation in mammals. *Curr. Opin. Genet. Dev.* **2017**, *43*, 120−127.
(62) Joest, E. F.; Winter, C.; Wesalo, J. S.; Deiters, A.; Tampé, R. Light-guided intrabodies for on-demand in situ target recognition in human cells. *Chem. Sci.* **2021**, *12*, 5787−5795.
(63) Kirchhofer, A.; Helma, J.; Schmidthals, K.; Frauer, C.; Cui, S.; Karcher, A.; Pellis, M.; Muyldermans, S.; Casas-Delucchi, C. S.; Cardoso, M. C.; Leonhardt, H.; Hopfner, K.-P.; Rothbauer, U. Modulation of protein properties in living cells using nanobodies. *Nat. Struct. Mol. Biol.* **2010**, *17*, 133−138.
(64) Kubala, M. H.; Kovtun, O.; Alexandrov, K.; Collins, B. M. Structural and thermodynamic analysis of the GFP:GFP-nanobody complex. *Protein Sci.* **2010**, *19*, 2389−2401.
(65) Schmied, W. H.; Elsässer, S. J.; Uttamapinant, C.; Chin, J. W. Efficient multisite unnatural amino acid incorporation in mammalian cells via optimized pyrrolysyl tRNA synthetase/tRNA expression and engineered eRF1. *J. Am. Chem. Soc.* **2014**, *136*, 15577−15583.
(66) Aloush, N.; Schvartz, T.; König, A. I.; Cohen, S.; Brozgol, E.; Tam, B.; Nachmias, D.; Ben-David, O.; Garini, Y.; Elia, N.; Arbely, E. Live cell imaging of bioorthogonally labelled proteins generated with a single pyrrolysine tRNA gene. *Sci. Rep.* **2018**, *8*, 14527.
(67) Zhou, W.; Wesalo, J. S.; Liu, J.; Deiters, A. Genetic code expansion in mammalian cells: A plasmid system comparison. *Bioorg. Med. Chem.* **2020**, *28*, 115772.
(68) Blees, A.; Januliene, D.; Hofmann, T.; Koller, N.; Schmidt, C.; Trowitzsch, S.; Moeller, A.; Tampé, R. Structure of the human MHC-I peptide-loading complex. *Nature* **2017**, *551*, 525−528.
(69) Fischbach, H.; Döring, M.; Nikles, D.; Lehnert, E.; Baldauf, C.; Kalinke, U.; Tampé, R. Ultrasensitive quantification of TAP-dependent antigen compartmentalization in scarce primary immune cell subsets. *Nat. Commun.* **2015**, *6*, 6199.
(70) Donnelly, M. L. L.; Luke, G.; Mehrotra, A.; Li, X.; Hughes, L. E.; Gani, D.; Ryan, M. D. Analysis of the aphthovirus 2A/2B polyprotein 'cleavage'mechanism indicates not a proteolytic reaction, but a novel translational effect: a putative ribosomal 'skip. *J. Gen. Virol.* **2001**, *82*, 1013−1025.
(71) Karginov, T. A.; Pastor, D. P. H.; Semler, B. L.; Gomez, C. M. Mammalian polycistronic mRNAs and disease. *Trends Genet.* **2017**, *33*, 129−142.
(72) Takimoto, J. K.; Xiang, Z.; Kang, J.-Y.; Wang, L. Esterification of an unnatural amino acid structurally deviating from canonical amino acids promotes its uptake and incorporation into proteins in mammalian cells. *ChemBioChem* **2010**, *11*, 2268−2272.
(73) Zhou, H.; Cheung, J. W.; Carpenter, T.; Jones, S. K., Jr.; Luong, N. H.; Tran, N. C.; Jacobs, S. E.; Galbada Liyanage, S. A.; Cropp, T. A.; Yin, J. Enhancing the incorporation of lysine derivatives into proteins with methylester forms of unnatural amino acids. *Bioorg. Med. Chem. Lett.* **2020**, *30*, 126876.
(74) Chan, L. Y.; Mugler, C. F.; Heinrich, S.; Vallotton, P.; Weis, K. Non-invasive measurement of mRNA decay reveals translation initiation as the major determinant of mRNA stability. *eLife* **2018**, *7*, No. e32536.
(75) Segal, I.; Nachmias, D.; Konig, A.; Alon, A.; Arbely, E.; Elia, N. A straightforward approach for bioorthogonal labeling of proteins and organelles in live mammalian cells, using a short peptide tag. *BMC Biol.* **2020**, *18*, 5.
(76) Lafranchi, L.; Schlesinger, D.; Kimler, K. J.; Elsässer, S. J. Universal Single-Residue Terminal Labels for Fluorescent Live Cell Imaging of Microproteins. *J. Am. Chem. Soc.* **2020**, *142*, 20080−20087.
(77) Wesalo, J. S.; Luo, J.; Morihiro, K.; Liu, J.; Deiters, A. Phosphine-activated lLysine analogues for fast chemical control of protein subcellular localization and protein SUMOylation. *ChemBioChem* **2020**, *21*, 141−148.
(78) Lerch, M. M.; Hansen, M. J.; van Dam, G. M.; Szymanski, W.; Feringa, B. L. Emerging targets in photopharmacology. *Angew. Chem., Int. Ed.* **2016**, *55*, 10978−10999.
(79) Hüll, K.; Morstein, J.; Trauner, D. In vivo photopharmacology. *Chem. Rev.* **2018**, *118*, 10710−10747.
(80) VanBrunt, M. P.; Shanebeck, K.; Caldwell, Z.; Johnson, J.; Thompson, P.; Martin, T.; Dong, H.; Li, G.; Xu, H.; D'Hooge, F.; Masterson, L.; Bariola, P.; Tiberghien, A.; Ezeadi, E.; Williams, D. G.; Hartley, J. A.; Howard, P. W.; Grabstein, K. H.; Bowen, M. A.; Marelli, M. Genetically encoded azide containing amino acid in mammalian cells enables site-specific antibody-drug conjugates using Click cycloaddition chemistry. *Bioconjugate Chem.* **2015**, *26*, 2249−2260.
(81) Roy, G.; Reier, J.; Garcia, A.; Martin, T.; Rice, M.; Wang, J.; Prophet, M.; Christie, R.; Dall'Acqua, W.; Ahuja, S.; Bowen, M. A.;

https://doi.org/10.1021/acssynbio.1c00471
ACS Synth. Biol. 2022, 11, 1466−1476

Marelli, M. Development of a high yielding expression platform for the introduction of non-natural amino acids in protein sequences. *MAbs* **2020**, *12*, 1684749.
(82) Klein, A.; Hank, S.; Raulf, A.; Joest, E. F.; Tissen, F.; Heilemann, M.; Wieneke, R.; Tampé, R. Live-cell labeling of endogenous proteins with nanometer precision by transduced nanobodies. *Chem. Sci.* **2018**, *9*, 7835−7842.
(83) Tietze, L. F.; Müller, M.; Duefert, S.-C.; Schmuck, K.; Schuberth, I. Photoactivatable prodrugs of highly potent duocarmycin analogues for a selective cancer therapy. *Chemistry* **2013**, *19*, 1726−1731.
(84) Uphoff, C. C.; Drexler, H. G. Detection of mycoplasma contamination in cell cultures. *Curr. Protoc. Mol. Biol.* **2014**, *106*, 28.4.1−28.4.14.

https://doi.org/10.1021/acssynbio.1c00471
ACS Synth. Biol. 2022, 11, 1466−1476